Catalytic microrotor driven by geometrical asymmetry

Mingcheng Yang, Marisol Ripoll, and Ke Chen

Citation: The Journal of Chemical Physics **142**, 054902 (2015); doi: 10.1063/1.4906823
View online: http://dx.doi.org/10.1063/1.4906823
View Table of Contents: http://scitation.aip.org/content/aip/journal/jcp/142/5?ver=pdfcov
Published by the AIP Publishing

Catalytic microrotor driven by geometrical asymmetry

Mingcheng Yang,[1,a)] Marisol Ripoll,[2] and Ke Chen[1]
[1]*Beijing National Laboratory for Condensed Matter Physics and Key Laboratory of Soft Matter Physics, Institute of Physics, Chinese Academy of Sciences, Beijing 100190, China*
[2]*Theoretical Soft-Matter and Biophysics, Institute of Complex Systems, Forschungszentrum Jülich, 52425 Jülich, Germany*

(Received 10 November 2014; accepted 15 January 2015; published online 3 February 2015)

An asymmetric gear with homogeneous surface properties is, here, presented as a prototype to fabricate catalytic microrotors. The driving torque arises from the diffusiophoretic effect induced by the concentration gradients generated by catalytic chemical reactions at the gear surface. This torque produces a spontaneous and unidirectional rotation of the asymmetric gear. By means of mesoscopic simulations, we prove and characterize this scenario. The gear rotational velocity is determined by the gear-solvent interactions, the gear geometry, the solvent viscosity, and the catalytic reaction ratio. Our work presents a simple way to design self-propelled microrotors, alternative to existing catalytic bi-component, or thermophoretic ones. © *2015 AIP Publishing LLC*. [http://dx.doi.org/10.1063/1.4906823]

I. INTRODUCTION

Motors with sizes in the nano- and microscales are ubiquitous in nature. Relevant examples are motor proteins which play a crucial role in a large number of biological processes.[1] Such biological molecular motors are powered by chemical reactions, typically hydrolysis of adenosine triphosphate (ATP). Inspired by nature, synthetic micromotors have, recently, been realized with chemical reactions catalyzed at the motor surfaces,[2–8] which convert chemical energy into mechanical work. The driving mechanisms can be attributed to the electro- or diffusiophoretic effects,[2,9,10] which are induced by local concentration gradients of molecular solutes catalytically generated by the motors themselves. The catalytic synthetic micromotors are receiving significant attention due to their wide potential applications in microfluidics, biology, or medicine, besides their relevance in fundamental understanding of non-equilibrium active matter.[11–16]

Self-propelled microrotors are a particularly important subclass of micromotors,[3,17–23] which can, for example, be used to power other microscale devices. Until now, all designs of the catalytic microrotors have considered systems with heterogeneous surface properties. In these cases, non-catalytic and catalytic materials are combined with precise dispositions resulting in a net rotational motion. This is the case of partially coated catalytic gears,[17] or of tethered twin Janus particles.[22] The material inhomogeneity breaks spatial symmetry, which is essential for the self-propelled motion.[24] Based on thermophoresis, a different strategy has recently been shown to be useful for the same purpose.[25] The idea is that a thermophoretic structure with a homogeneous surface but a non-symmetric geometry is sufficient to produce a self-propelled rotation. Moreover, two recent theoretical works have proposed that catalytic particles with shape-anisotropy only can experience self-propelled translation.[26,27] An important question is, thus, whether a similar design is feasible for catalytic microrotors.

In this paper, we show that a geometrically asymmetric microgear with a homogeneous catalytic surface can spontaneously and unidirectionally rotate in a solvent. The driving torque arises from the non-symmetric diffusiophoretic forces exerted on the gear edges by catalytically induced concentration gradient of the reactant molecules. The validity of this proposed model is justified by performing mesoscopic molecular simulations. The speed and direction of the self-propelled rotation are determined by the gear geometry, the interactions with the solvent, and the catalytic reaction probability. This purely geometrical strategy provides a deeper insight into synthetic micro-devices, and opens an alternative and simple route to design catalytic self-propelled microrotors, which can be relatively easily manufactured.

II. SIMULATION MODEL AND METHOD

We perform computer simulations to study the motion of an asymmetric microgear with a homogeneous catalytic surface (Fig. 1). For simplicity, we consider a fully two dimensional system. A particle-based hybrid scheme of dynamic simulations provides a mesoscopic description of both the solvent and the gear, with tunable interactions. The simulation scheme follows closely the one employed for the self-propelled thermophoretic microgear.[25] The solvent is modeled with multiparticle collision dynamics (MPC),[28–33] while the microgear and the gear-solvent interactions are simulated by standard molecular dynamics (MD). In MPC, the solvent is modeled as a large number N of point particles of mass m with continuous positions and velocities. The MPC dynamics consists of alternate streaming and collision steps. In the streaming step, each solvent particle moves ballistically for a fixed time h. In the collision step, particles are sorted into square cells of size a, and interact only with members of their own cell. In the simulations, we use the stochastic rotation

[a)]Electronic address: mcyang@iphy.ac.cn

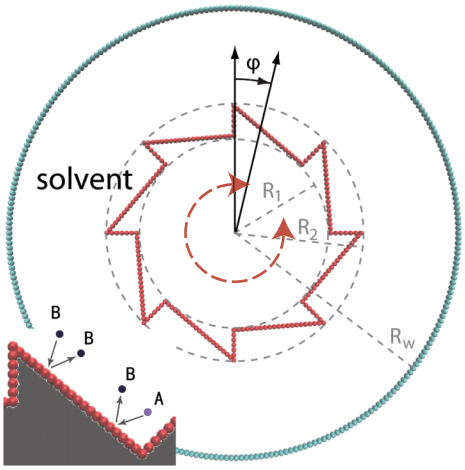

FIG. 1. Sketch of the simulation setup of the eight-tooth microgear within a circular wall. Inset depicts the chemical reaction from A to B catalyzed by the edges of the microgear.

collision rule with variable collision angle α introduced by Ryder and Yeomans.[25,34] This collision rule locally conserves mass, linear momentum, energy, and also angular momentum. This ensures that the algorithm properly captures hydrodynamic behaviors, thermal fluctuations, and mass diffusion. Furthermore, the angular momentum conservation ensures the correctness of the rotation dynamics. Reduced simulation units are employed by setting $a = 1$, the particle mass $m = 1$, and $k_BT = 1$, with k_B being the Boltzmann constant and T the system temperature. The chosen MPC parameters are $h = 0.1$, and the mean number of solvent particles per cell $\rho = 10$. Although no specific kinetic theory is developed for this collision rule, an approximation to the kinetic theory of MPC with fixed collision angle $\alpha = 90$,[35] predicts the Schmidt number to be $Sc \simeq 12$, which corresponds to a liquid-like behavior.

The microgear model used here consists of two elements. One is a rigid gear with eight teeth. This rigid gear has an internal radius $R_1 = 19$, an external radius $R_2 = 25$, and a moment of inertia $I = 10^6$, and is free to rotate around its center that is fixed in space. Then a single-layer of monomer beads is mounted along the rigid gear edges and linked to it by a harmonic spring of constant $k = 600$, as depicted in Fig. 1. The separation between neighboring beads is 1 and no direct interactions exist between them. The microgear is surrounded by MPC solvent confined inside a circular outer wall with radius $R_w = 45$, which is constructed by fixing beads with springs along an external circle. The beads on the gear and the external wall interact with the solvent particles through a repulsive Lennard-Jones (LJ) type potential[36,37]

$$U_k(r) = 4\epsilon\left[\left(\frac{\sigma}{r}\right)^{2n} - \left(\frac{\sigma}{r}\right)^{n}\right] + \epsilon, \mathbf{r} \le r_c. \qquad (1)$$

Here, r is the distance between the bead center and the solvent particle, the cutoff $r_c = \sqrt[n]{2}\sigma$, ϵ refers to the potential intensity, σ to the bead radius, n to a positive integer number, and k to the solvent particle species in a multi-component solvent. The bead radius is taken as $\sigma = 1.25$, such that the large overlap between neighboring beads prevents the solvent particles (not shown in Fig. 1) from penetrating the microgear or the outer wall. The range and stiffness of the potential are determined by parameters (n, ϵ), thus, we denote $U_k(n, \epsilon)$ as the potential of the k species. For a fixed n, larger ϵ implies steeper potential and hence a stronger repulsive interaction. For a fixed ϵ, larger n also implies steeper potential, but together with a considerably smaller interaction range, which effectively corresponds to an overall weaker repulsion. Note that the rigid gear (only used to fix the relative equilibrium positions of the beads on the microgear) does not directly interact with the MPC solvent, and the torque on the rigid gear is transferred through the linked beads. The equations of motion for both the rigid gear and the linked beads are integrated with a velocity-Verlet MD algorithm with a time step $\Delta t = h/50$. We point out that the scheme to construct a microgear is not unique, but our present method combining the rigid gear with the surface beads is particularly simple, in which the bead-solvent potential interactions can produce a strong diffusiophoretic effect.

To model catalytic chemical reactions, we follow the route already used in previous simulation studies of chemically powered microswimmers.[38–41] The solvent is simulated as a mixture of two species, A and B, whose only differences lie in the interaction with the gear surface beads, $U_A(n, \epsilon)$ and $U_B(n', \epsilon')$. Both A and B solvent particles participate in the MPC collisions, in which particle types are not distinguished. Furthermore, whenever an A-type particle interacts with the gear beads, the reaction $A + C \rightarrow B + C$ occurs with a probability P_r (see inset of Fig. 1), e.g., decomposition of the hydrogen peroxide into oxygen and water. The change of potential energy at the reaction site can lead to local heating of the surrounding solvent. In order to avoid this effect and to model a purely diffusiophoretic rotor, the catalytic reaction is only implemented for those A-type particles, which had collided with the gear and have just come out from the interaction areas of both U_A and U_B. This ensures a chemical reaction without an energy jump.[42]

The chemical reaction catalyzed by the gear is irreversible, such that A-type solvent particles are gradually consumed. In order to keep a stationary concentration gradient, A-type particles need to be constantly fed into the system. We initialize the simulations with a solvent composed completely of A-type particles, and whenever a B-type particle collides with the external wall, it automatically converts into A. The precise interaction of both species with the beads of the external wall is not relevant, and we choose the same potential $U_k(24, 1)$ for both species.

III. RESULTS AND DISCUSSION

After switching on the catalytic reaction, the reaction product (i.e., B-type particles) diffuses away from the gear surface, and a steady-state concentration distribution is quickly established. Figure 2 displays the steady-state distribution of concentration fraction of B-type solvent, ρ_B/ρ. This concentration is measured by keeping the microgear completely fixed. Reactant solvent particles (A-type) close to the cleft of each gear tooth encounter a larger catalytic area than those close to the summit. The different size of the

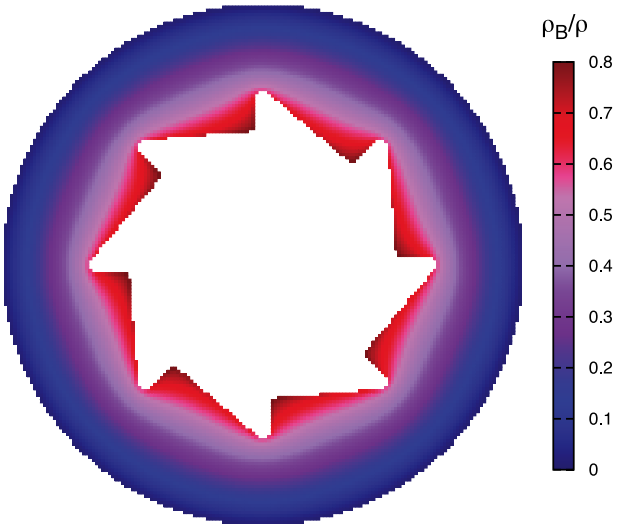

FIG. 2. Product concentration fraction distribution ρ_B/ρ in the steady state. The employed gear-solvent interactions have $Pr = 0.02$, $U_A(3,1)$, and $U_B(24,1)$.

catalytic areas leads to different production rate of B-type particles along the edges. This is a purely geometrical effect which induces concentration gradients of the reaction product along the short edge ∇c_s, and the long edge ∇c_l of each gear tooth, as shown in Fig. 2. The precise values of the gradients depend on the geometry (angles and lengths of the gear teeth), and on the reaction probability P_r.

The self-generated concentration gradients around catalytic microdimers[38–40] or Janus particles[41,43] has already been shown to be able to produce self-propelled motion. This motion can be understood as a result of a *diffusiophoretic force* $\mathbf{f}_c$ which arises from the interactions between the particles and the inhomogeneous solvent environment. The diffusiophoretic force is proportional to the gradient of product concentration $\mathbf{f}_c \sim \nabla c$. In the case of the catalytic microgear, the concentration gradients ∇c_l and ∇c_s induces diffusiophoretic forces $\mathbf{f}_{c,l}$ and $\mathbf{f}_{c,s}$ along the long and short edges of each gear tooth. This exerts a non-vanishing torque $\mathcal{T} \sim \Sigma(\mathbf{R}_l \times \mathbf{f}_{c,l} + \mathbf{R}_s \times \mathbf{f}_{c,s})$ on the gear. Here, $\mathbf{R}_l$ and $\mathbf{R}_s$, respectively, refer to the coordinates of the center of force on the long and short edges, and the summation accounts for multiple teeth. For the gear in Fig. 1 (also in most of our simulations), the short tooth edge (hence $\mathbf{R}_s$) is parallel to the radial direction, and the long tooth edge is perpendicular to the corresponding short edge at the cleft. This means that only the diffusiophoretic forces applied on the long edges contribute to the total torque, $\mathcal{T} \propto (\mathbf{R}_l \times \mathbf{f}_{c,l})$. On the other hand, besides the diffusiophoretic forces, the solvent also exerts pressure forces normal to the gear edges. The pressure forces on the short and long edges of the gear teeth produce torques in opposite directions that cancel each other, thus do not contribute to the driving torque. The steady-state rotational velocity of the microgear is calculated as

$$\omega = N\mu_r \mathbf{R}_l \times \mathbf{f}_{c,l}, \tag{2}$$

where μ_r is the rotational mobility and N the number of teeth of the microgear. Thus, the self-propelled rotation of the catalytic gear is clearly determined by the diffusiophoretic properties of the gear.

The rotation of the microgear is characterized by quantifying the rotational angle φ. As illustrated in Fig. 1, a positive φ is defined as a clockwise rotation. Simulation results averaged over a minimum of 8 independent runs are plotted in Fig. 3. The asymmetric catalytic gear clearly rotates around its center, whose rotational speed and direction depend on the gear-solvent interactions, U_A and U_B. The inset in Fig. 3 displays an instantaneous rotation trajectory (also see (Multimedia view)), which shows that the self-propelled rotation is accompanied by thermal fluctuations. In these simulations, we fix the reaction probability at $Pr = 0.02$, and choose four different gear-solvent couplings: (I) $U_A(3,1)$, $U_B(24,1)$; (II) $U_A(24,1)$, $U_B(3,1)$; (III) $U_A(3,1)$, $U_B(3,2)$; and (IV) $U_A(3,1)$, $U_B(3,0.5)$. Microgears with couplings I and IV show a clockwise rotation, while microgears with couplings II and III experience a counterclockwise rotation. Given the type of coupling used in our simulations, this trend can be intuitively understood by considering that the diffusiophoretic force $\mathbf{f}_c$ is directed toward the area where the enriched component has weaker repulsion. This is in agreement with the trend, already, observed in simulations of catalytic dimers.[38,39,44] Accounting for more general concepts in diffusiophoretic phenomena, the rotational direction is related to the variation of surface energy induced by ∇c_l. The solvent layer close to the microgear can be regarded as an interface separating the bulk solvent and the microgear. Longer interaction range and larger potential intensity lead, in general, to higher surface energy. In the cases of couplings I and IV, the surface energy decreases with the concentration of B-type particles, such that the directions of $\mathbf{f}_{c,l}$ and ∇c_l are the same, hence clockwise rotations. In the cases of II and III, the situation is reversed. Note that the couplings I and II are completely symmetric, although their rotational velocities are not exactly opposite since the reactant and product concentrations are not necessarily the same.

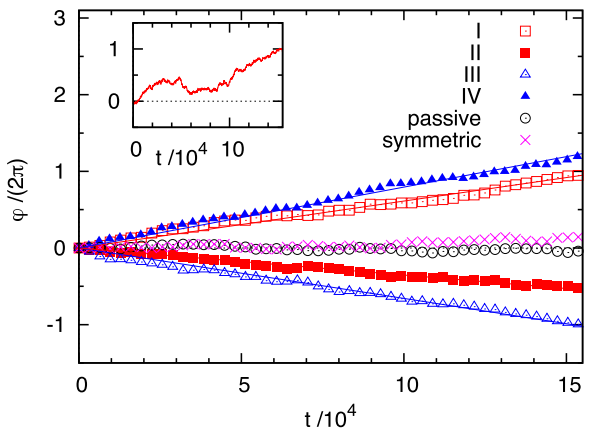

FIG. 3. Averaged time evolution of the microgear rotational angle. Symbols denote simulation results and lines linear fits. The reaction probability is fixed to $P_r = 0.02$, and various gear-solvent interactions (I-IV) are used. Circles refer to a non-catalytic gear (`passive`), and crosses to a symmetric gear (`symmetric`). Inset is a single run with coupling I, with its corresponding movie given. (Multimedia view) [URL: http://dx.doi.org/10.1063/1.4906823.1].

In all cases, the self-induced rotation is due to the breakdown of the spatial symmetry of the catalytic gear. To test this argument, we perform additional simulations for a gear with symmetric profile. The result shows a vanishing net rotation (Fig. 3). In this case, the diffusiophoretic forces along both sides of each tooth are symmetric with respect to the microgear radial direction, which results in a zero torque. For comparison, we also simulate a passive (non-catalytic) gear, where no net rotation is observed either.

The rotational velocity ω is determined by $\mathbf{f}_{c,l}$, as shown in Eq. (2), and it will, therefore, be proportional to the gradient of product concentration along the long edge of each gear tooth. To verify this relation, we vary the product concentration gradient by changing the catalytic reaction probability P_r. Figure 4 shows the angular velocity ω of an asymmetric gear as a function of the product concentration gradient ∇c_l for a fixed gear-solvent interaction. Besides statistical uncertainty, the results convincingly prove the linear relation $\omega \sim \nabla c_l$. The inset of Fig. 4 shows that ∇c_l has a maximum around $P_r = 0.02$. This is easy to understand since for $P_r = 0$ there is no catalytic reaction and therefore no reaction product (passive gear); while, for $P_r = 1$, the reaction is so fast that the product particles will almost occupy the whole boundary layer near the gear resulting in an almost vanishing gradient within the boundary layer. Both limits translate into a negligible rotational speed.

In our simulations, finite size effects given by the outer wall are ignored based on the following considerations. The gear motion is determined by the local concentration gradients near the gear edges. Under the condition of constant flux of reaction product on the gear surface, which is the case for the low reaction rates employed in our simulations, the local concentration gradients near the gear are independent of the distance to the outer wall. On the other hand, the velocity field induced by the 2D active gear decays faster than that of a passive gear, such that hydrodynamic finite size effects are also relatively weak.

Finally, we give an estimation of the order of magnitude of the microgear rotational speed to demonstrate its experimental feasibility. In our simulations, the gear size is much larger than the solvent-gear interaction length, which corresponds to a microscale gear immersed in a simple liquid for experiments. Thus, we consider a 3-dimensional catalytic micron-sized gear of external radius $R_2 = 8\ \mu$m and thickness $h_H = 1\ \mu$m. Its rotational mobility can be calculated as $\mu_r = 1/(4\pi\eta R_2^2 h_H)$,[45] with η being the solvent viscosity. On the other hand, it is known that a half-platinum-coated polystyrene Janus particle with a radius of 0.8 μm has a typical self-propelled speed $u \sim 1\ \mu\text{m s}^{-1}$ in hydrogen peroxide solutions.[4] Thus, the diffusiophoretic driving force can be approximated by $\mathbf{f}_c \sim 4.8\pi\eta u$, where the Stokes friction is considered. Assuming that the diffusiophoretic force exerted on a long edge of the catalytic microgear has a similar magnitude, the torque on a gear with the geometry of Fig. 1 becomes $\mathcal{T} \sim 8R_2\mathbf{f}_c$, where the approximation $R_l \simeq R_2$ is considered. The rotational speed can be estimated as $\omega \sim \mu_r\mathcal{T} \simeq 0.2$ rounds per second, which is of the same order of magnitude as for partially coated catalytic gears in Ref. 17. The active rotation of such catalytic microgears would be easily observed in experiments.

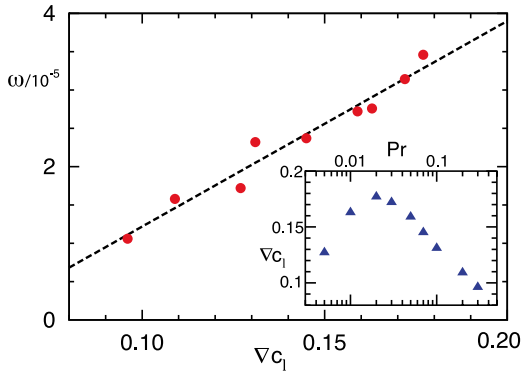

FIG. 4. Rotational velocity ω of the asymmetric catalytic microgear as a function of the product concentration gradient along the long edge ∇c_l. Here, coupling I is fixed for the gear-solvent interaction and Pr is varied. Inset: variation of ∇c_l with Pr.

IV. CONCLUSIONS

In this work, we have presented a simple self-propelled catalytic microrotor composed of a geometrically asymmetric gear with uniform material properties immersed in a solution. The uni-directional rotation of the microgear is driven by the diffusiophoretic forces exerted on the microgear edges, which arise from the catalytically induced concentration gradient of the solute molecules due to purely geometrical effect of the microgear. We have performed mesoscopic simulations to justify the proposed model. The results indicate that the rotational speed and direction of the microgear can be easily tuned by changing the gear-solvent interactions, the gear geometry, or the catalytic reaction probability on the gear surface. Our findings provide an alternative and simple strategy to design synthetic catalytic micromotors, which could have many potential applications in fields like microfluidics and biomedicine.

ACKNOWLEDGMENTS

M.Y. gratefully acknowledges support from the National Natural Science Foundation of China (Grant No. 11404379). K.C. gratefully acknowledges the support from National Science Foundation of China (Grant No. 11474327) and the "The Recruitment Program of Global Youth Experts" from the government of China. This work was also supported by the MOST 973 Program (No. 2015CB856800).

[1]F. Jülicher, A. Ajdari, and J. Prost, Rev. Mod. Phys. **69**, 1269 (1997).
[2]W. F. Paxton, K. C. Kistler, C. C. Olmeda, A. Sen, S. K. S. Angelo, Y. Cao, T. E. Mallouk, P. E. Lammert, and V. H. Crespi, J. Am. Chem. Soc. **126**, 13424 (2004).
[3]S. Fournier-Bidoz, A. C. Arsenault, I. Manners, and G. A. Ozin, Chem. Commun. **2005**, 441–443.
[4]J. R. Howse, R. A. L. Jones, A. J. Ryan, T. Gough, R. Vafabakhsh, and R. Golestanian, Phys. Rev. Lett. **99**, 048102 (2007).
[5]L. F. Valadares, Y. G. Tao, N. S. Zacharia, V. Kitaev, F. Galembeck, R. Kapral, and G. A. Ozin, Small **6**, 565 (2010).
[6]T. Mirkovic, N. S. Zacharia, G. D. Scholes, and G. A. Ozin, Small **6**, 159 (2010).
[7]J. Gibbs and Y. Zhao, Front. Mater. Sci. **5**, 25 (2011).
[8]S. Sengupta, M. E. Ibele, and A. Sen, Angew. Chem., Int. Ed. **51**, 8434 (2012).

[9]J. L. Anderson, Annu. Rev. Fluid Mech. **21**, 61 (1989).
[10]R. Golestanian, T. B. Liverpool, and A. Ajdari, Phys. Rev. Lett. **94**, 220801 (2005).
[11]Y. Hong, N. M. K. Blackman, N. D. Kopp, A. Sen, and D. Velegol, Phys. Rev. Lett. **99**, 178103 (2007).
[12]J. Palacci, C. Cottin-Bizonne, C. Ybert, and L. Bocquet, Phys. Rev. Lett. **105**, 088304 (2010).
[13]I. Theurkauff, C. Cottin-Bizonne, J. Palacci, C. Ybert, and L. Bocquet, Phys. Rev. Lett. **108**, 268303 (2012).
[14]W. Wang, W. Duan, A. Sen, and T. E. Mallouk, Proc. Natl. Acad. Sci. U. S. A. **110**, 17744 (2013).
[15]J. Palacci, S. Sacanna, A. P. Steinberg, D. J. Pine, and P. M. Chaikin, Science **339**, 936 (2013).
[16]A. A. Solovev, S. Sanchez, and O. G. Schmidt, Nanoscale **5**, 1284 (2013).
[17]J. M. Catchmark, S. Subramanian, and A. Sen, Small **1**, 202 (2005).
[18]Y. He, J. Wu, and Y. Zhao, Nano Lett. **7**, 1369 (2007).
[19]L. Qin, M. J. Banholzer, X. Xu, L. Huang, and C. A. Mirkin, J. Am. Chem. Soc. **129**, 14870 (2007).
[20]Z. Fattah, G. Loget, V. Lapeyre, P. Garrigue, C. Warakulwit, J. Limtrakul, L. Bouffier, and A. Kuhn, Electrochim. Acta **56**, 10562 (2011).
[21]Y. Wang, S. Fei, Y. Byun, P. E. Lammert, V. H. Crespi, A. Sen, and T. E. Mallouk, J. Am. Chem. Soc. **131**, 9926 (2009).
[22]S. Ebbens, R. A. L. Jones, A. J. Ryan, R. Golestanian, and J. R. Howse, Phys. Rev. E **82**, 015304(R) (2010).
[23]J. Gibbs, S. Kothari, D. Saintillan, and Y. Zhao, Nano Lett. **11**, 25430 (2011).
[24]R. Feynman, *The Feynman Lectures on Physics* (Addison-Wesley, Reading, 1963).
[25]M. Yang and M. Ripoll, Soft Matter **10**, 1006 (2014).
[26]S. Shklyaev, J. F. Brady, and U. M. Córdova-Figueroa, J. Fluid Mech. **748**, 488 (2014).
[27]H. H. Wei and J. S. Jan, J. Fluid Mech. **657**, 64 (2010).
[28]A. Malevanets and R. Kapral, J. Chem. Phys. **110**, 8605 (1999).
[29]M. Ripoll, K. Mussawisade, R. G. Winkler, and G. Gompper, Phys. Rev. E **72**, 016701 (2005).
[30]J. T. Padding and A. A. Louis, Phys. Rev. E **74**, 031402 (2006).
[31]R. Kapral, Adv. Chem. Phys. **140**, 89 (2008).
[32]G. Gompper, T. Ihle, D. M. Kroll, and R. G. Winkler, Adv. Polym. Sci. **221**, 1 (2009).
[33]M. Yang and M. Ripoll, Phys. Rev. E **84**, 061401 (2011).
[34]J. F. Ryder, "Mesoscopic simulations of complex fluids," Ph.D. thesis, University of Oxford, 2005.
[35]E. Tüzel, T. Ihle, and D. M. Kroll, Phys. Rev. E **74**, 056702 (2006).
[36]G. A. Vliegenthart, J. F. M. Lodge, and H. N. W. Lekkerkerker, Physica A **263**, 378 (1999).
[37]D. Lüsebrink, M. Yang, and M. Ripoll, J. Phys.: Condens. Matter **24**, 284132 (2012).
[38]G. Rückner and R. Kapral, Phys. Rev. Lett. **98**, 150603 (2007).
[39]Y. G. Tao and R. Kapral, J. Chem. Phys. **128**, 164518 (2008).
[40]Y. G. Tao and R. Kapral, Soft Matter **6**, 756 (2010).
[41]M. Yang, A. Wysocki, and M. Ripoll, Soft Matter **10**, 6208 (2014).
[42]Note that other strategies are also possible. One is to choose the potentials of the two species to be identical in the interaction range, as in Ref. 41. Another one is to allow for the local heating effect to occur and account for the self-propelled motion as the sum of the diffusiophoretic and thermophoretic effects.[38,43]
[43]P. de Buyl and R. Kapral, Nanoscale **5**, 1337 (2013).
[44]Note that in Ref. 38 there is a misprint in the definition of the dimer direction which has been corrected in subsequent publications of the same authors.[39]
[45]P. G. Saffman and M. Delbrück, Proc. Natl. Acad. Sci. U. S. A. **72**, 3111 (1975).